JOURNAL OF PROPULSION AND POWER
Vol. 9, No. 4, July–Aug. 1993

Inviscid Finite-Volume Lambda Formulation

Francesco Casalini* and Andrea Dadone†
Politecnico di Bari, Bari 70125, Italy

A finite-volume lambda formulation for solving Euler equations and able to handle compressible as well as transonic flow computations is presented. The easy extension of the methodology to the solution of Navier-Stokes equations is indicated. The integration scheme is in nonconservative form in smooth flow regions in order to take advantage of its superior accuracy and computational efficiency. It automatically switches to conservative form in shock regions, in order to capture them correctly. Computations of two- and three-dimensional shockless source flows prove the superior accuracy and computational efficiency of the proposed technique in comparison with a classical conservative upwind methodology. Moreover, computed results referring to some two- and three-dimensional test cases are compared with numerical or experimental published ones, thus showing the capabilities of the proposed formulation to deal with inviscid subsonic as well as transonic flow cases.

Nomenclature

a	=	speed of sound
C_p	=	pressure coefficient
e, h^0	=	total energy and total enthalpy per unit mass
e_i	=	right eigenvectors
$\boldsymbol{F}, \tilde{\boldsymbol{F}}$	=	flux vectors at a cell face
$\boldsymbol{f}, \boldsymbol{g}, \boldsymbol{h}$	=	inviscid flux vectors
$\underline{i}_x, \underline{i}_y, \underline{i}_z$	=	unit vectors in the x, y, z directions
k_x, k_y, k_z	=	direction cosines to the cell face normal
l_x, l_y, l_z	=	direction cosines of the first vector tangent to the cell face
m_x, m_y, m_z	=	direction cosines of the second vector tangent to the cell face
$\underline{n}$	=	unit vector normal to the cell face
p, p_a	=	local and outlet (atmospheric) static pressure
p_t, p_T	=	local and tank total pressure
$\boldsymbol{q}$	=	vector of conserved variables
$\hat{q}$	=	average of vector $\boldsymbol{q}$ in a finite volume
r	=	radial distance from the origin
T	=	transformation matrix
u, v, w	=	components of the velocity vector in the x, y, z directions
$\tilde{u}$	=	velocity component normal to the cell face
$\tilde{v}, \tilde{w}$	=	velocity components parallel to a set of arbitrarily defined tangent vectors in the plane of the cell face
v_r	=	radial velocity component
x, y, z	=	Cartesian coordinates
ΔS	=	surface area
ΔV	=	volume of the considered finite volume
δ	=	difference operator, i.e., difference of some property between two cell faces characterized by the same generalized coordinate
λ_i	=	eigenvalues
ξ, η, ζ	=	generalized coordinates
ρ	=	density

Subscripts

t	=	partial derivative with respect to time
x, y, z	=	partial derivative with respect to coordinates x, y, z

Superscript

—	=	average value to be evaluated at the cell center

Presented as Paper 91-2258 at the AIAA/SAE/ASME 27th Joint Propulsion Conference, Sacramento, CA, June 24–26, 1991; received March 2, 1992; revision received Jan. 15, 1993; accepted for publication Jan. 21, 1993.

*Associate Professor, Istituto di Macchine ed Energetica, Via Re David 200.

†Professor, Istituto di Macchine ed Energetica. Senior Member AIAA.

Introduction

THIS article is concerned with the numerical simulation of inviscid flows and aims to improve and refurbish the classical lambda formulation.[1] Such an approach presents several, very desirable features: coding simplicity, solution accuracy, and low computing time per integration step. Owing to its inherently nonconservative framework, the lambda formulation requires special shock wave treatments which can be classified into two fundamentally different procedures:

1) The shock-fitting technique[2]: shock waves are computed by means of an explicit enforcement of Rankine-Hugoniot conditions at the shock front. In spite of its theoretical skillfulness and many interesting results obtained for two- and three-dimensional steady as well as unsteady flows,[3–6] such a technique has not been extended to complex geometries, although this extension is feasible in principle.

2) The hybrid formulations[7–9]: shock waves are captured by the three different types of suggested hybrid formulations, either by inserting appropriate correction terms into the classical lambda formulation in order to restore a correct coupling between the supersonic flow region and the shocked subsonic one, or by switching from the classical lambda formulation to a flux difference or a flux vector splitting methodology in the shock transition region. These techniques are hybrid because they take use of different dependent variables in different regions of the flows.

Finally, it must be pointed out that the classical as well as the outlined hybrid lambda formulations are apt to finite-difference approximations, while finite-volume discretizations seem to be much more attractive when flows in complex geometries must be computed.

On the other hand, as found by Godunov,[10] upwind conservative methodologies automatically capture monotonic shocks if the employed numerical scheme is limited to a first-order space accuracy, which is generally unsatisfactory if used to compute the entire flowfield. In order to obtain monotonic and higher order space accurate results, the employed numerical scheme must selfadapt to the solution it generates, so that the automatic shock-capturing property is lost. Moreover, captured shocks are represented by a smooth transition

over some meshes so that, in order to reduce the "numerical shock thickness," a local mesh refinement is sometimes employed, which again causes the automatic shock-capturing capability to be lost. Finally, such methodologies handle some boundary conditions in a more difficult way, require a higher computational time with respect to the classical lambda formulation, and present a lower accuracy.

We may conclude that the conservative property is needed only to capture discontinuities, while nonconservative forms of the equations can be much more attractive in smooth regions, because of their advantages: higher computational efficiency, better accuracy, and simpler boundary conditions enforcement. Such a switching between conservative and nonconservative forms requires a shock detection device, which is needed by the shock-capturing conservative methodologies too, as above outlined. Accordingly, it seems a worthwhile attempt to refurbish the lambda formulation by developing an improved version apt to transonic flow computations in complex geometries, without being supplemented by a discontinuity fitting technique, and satisfying the following requirements: 1) equations discretized in nonconservative form in smooth flow regions; 2) conservative property automatically recovered near discontinuities; 3) use of the same dependent variables everywhere in the flowfield; 4) finite-volume formulation; and 5) preservation of the superior accuracy of the classical lambda formulation. Moreover, it seems advisable that the new formulation be in a form suitable for an easy extension to compute Navier-Stokes equations.

Reference 11 can be considered a first step in this direction: a one-dimensional version of an improved lambda formulation satisfying the previously outlined features has been suggested and tested vs steady as well as unsteady one-dimensional flows, proving the improved version to be characterized by a slightly superior accuracy with respect to the classical one. A multidimensional version has then been suggested in Ref. 12: the formulation and the computed results, referring to two- and three-dimensional source flows, are essentially limited to Cartesian meshes. The main objective of the paper was to prove the feasibility and simplicity of the conservative-nonconservative switching, for curved shocks, together with the superior accuracy of the improved lambda formulation in comparison with a flux difference splitting methodology.

This article first presents the finite-volume lambda formulation with reference to a general three-dimensional curvilinear coordinate system. Computed results referring to two- and three-dimensional shockless source flows are then presented, in order to prove the superior accuracy and computational efficiency of the proposed technique in comparison with a classical conservative upwind methodology. Finally, computed results pertaining to some two- and three-dimensional test cases are compared with numerical or experimental published ones, thus showing the capability of the proposed formulation to deal with inviscid subsonic as well as transonic flow cases. The formulation and most of the results here presented have been already reported in Ref. 13.

Governing Equations and Numerical Technique

The vector form of the Euler equations in a Cartesian coordinate system can be written as[14]

$$\boldsymbol{q}_t + \boldsymbol{f}_x + \boldsymbol{g}_y + \boldsymbol{h}_z = 0 \tag{1}$$

The vector of conserved variables and the inviscid flux vectors are given by

$$\boldsymbol{q} = [\rho, \rho u, \rho v, \rho w, \rho e]^T \tag{2}$$

$$\begin{aligned} \boldsymbol{f} &= [\rho u, p + \rho u^2, \rho uv, \rho uw, \rho uh^0]^T \\ \boldsymbol{g} &= [\rho v, \rho uv, p + \rho v^2, \rho vw, \rho vh^0]^T \\ \boldsymbol{h} &= [\rho w, \rho uw, \rho vw, p + \rho w^2, \rho wh^0]^T \end{aligned} \tag{3}$$

The extension of Eq. (1) to the Navier-Stokes equations can be easily obtained by subtracting the heat conduction and shear stress contributions from the corresponding flux vectors associated with the Euler equations.

Each unitary volume in the computational space corresponds to a finite volume with six faces in the physical space, each couple of faces being characterized by one of the three curvilinear lines corresponding to the coordinate lines in the computational space. With reference to such a volume, a semidiscrete finite-volume representation of Eq. (1) leads to

$$\Delta V \hat{q}_t + \sum [\delta(F \Delta S)] = 0 \tag{4}$$

where

$$F = (f\underline{i}_x + g\underline{i}_y + h\underline{i}_z) \cdot \underline{n} \tag{5}$$

It must be noticed that the summation implied in Eq. (4) must be extended to the three curvilinear directions corresponding to the coordinate system in the computational space.

According to Eq. (5), the fluxes at each face are given by

$$F = [\rho\tilde{u}, k_x p + \rho u\tilde{u}, k_y p + \rho v\tilde{u}, k_z p + \rho w\tilde{u}, \rho h^0 \tilde{u}]^T \tag{6}$$

being

$$\tilde{u} = k_x u + k_y v + k_z w \tag{7}$$

Such fluxes premultiplied by an appropriate matrix T, give

$$\tilde{F} = TF = [\rho\tilde{u}, p + \rho\tilde{u}^2, \rho\tilde{v}\tilde{u}, \rho\tilde{w}\tilde{u}, \rho h^0 \tilde{u}]^T \tag{8}$$

where

$$T = \begin{bmatrix} 1 & 0 & 0 & 0 & 0 \\ 0 & k_x & k_y & k_z & 0 \\ 0 & l_x & l_y & l_z & 0 \\ 0 & m_x & m_y & m_z & 0 \\ 0 & 0 & 0 & 0 & 1 \end{bmatrix} \tag{9}$$

$$T^{-1} = \begin{bmatrix} 1 & 0 & 0 & 0 & 0 \\ 0 & k_x & l_x & m_x & 0 \\ 0 & k_y & l_y & m_y & 0 \\ 0 & k_z & l_z & m_z & 0 \\ 0 & 0 & 0 & 0 & 1 \end{bmatrix} \tag{10}$$

$$\tilde{v} = l_x u + l_y v + l_z w \tag{11}$$

$$\tilde{w} = m_x u + m_y v + m_z w \tag{12}$$

Taking into account Eq. (8), Eq. (4) can be expressed as

$$\Delta V \hat{q}_t + \sum \delta[(T^{-1}\tilde{F})\Delta S] = 0 \tag{13}$$

or

$$\Delta V \hat{q}_t + \sum [(\overline{\Delta S T^{-1}})\delta\tilde{F} + \delta(\Delta S T^{-1})\bar{\tilde{F}}] = 0 \tag{14}$$

In Eq. (14), the contributions due to the flux variations are separated by those related to the geometry variations.

Flux difference splitting techniques give useful expression to relate the flux differences between the two sides of an interface (approximate solution of the corresponding Riemann problem). The same expressions can be here used to evaluate the difference of the fluxes between two faces characterized by the same curvilinear line, corresponding to one of the coordinate lines in the computational space. Flux difference splitting techniques solve the one-dimensional Riemann problem at the interface, while, at this stage, the present technique solves a one-dimensional Riemann problem be-

tween each couple of corresponding faces. Accordingly such a flux difference can be written as

$$\delta\bar{F} = \sum \alpha_i \lambda_i e_i \tag{15}$$

where

$$\alpha_1 = (\delta p + \rho a \delta\bar{u})/2a^2; \quad \alpha_2 = (\delta p - \rho a \delta\bar{u})/2a^2$$
$$\alpha_3 = \rho\delta\bar{v}; \quad \alpha_4 = \rho\delta\bar{w}; \quad \alpha_5 = \delta\rho - \delta p/a^2 \tag{16}$$

$$\lambda_1 = \bar{u} + a; \quad \lambda_2 = \bar{u} - a; \quad \lambda_3 = \lambda_4 = \lambda_5 = \bar{u} \tag{17}$$

$$q^2 = u^2 + v^2 + w^2 \tag{18}$$

and the right eigenvectors e_i are represented by the columns of the following matrix:

$$P = \begin{bmatrix} 1 & 1 & 0 & 0 & 1 \\ \bar{u} + a & \bar{u} - a & 0 & 0 & \bar{u} \\ \bar{v} & \bar{v} & 1 & 0 & \bar{v} \\ \bar{w} & \bar{w} & 0 & 1 & \bar{w} \\ h^0 + a\bar{u} & h^0 - a\bar{u} & \bar{v} & \bar{w} & q^2/2 \end{bmatrix} \tag{19}$$

At this stage the lambda formulation approximation is used: all the finite-differences in Eq. (16) are approximated by one-side differences taken between the mesh point at the center of the considered finite volume and the upstream mesh points, if the corresponding λ_i is positive, or the downstream mesh points, if the corresponding λ_i is negative. As an example, if $\delta\bar{F}$ represents a flux variation in the ξ direction and λ_i is positive, $\delta\bar{v}$ will be taken between the point $[n\Delta\xi, m\Delta\eta, 1\Delta\zeta]$, at the center of the considered finite volume, and the points $[(n-1)\Delta\xi, m\Delta\eta, 1\Delta\zeta]$ and $[(n-2)\Delta\xi, m\Delta\eta, 1\Delta\zeta]$, if a second-order spatial approximation is required. Moreover, the geometry variation terms in Eq. (14) are evaluated at the beginning of the computations by means of central differences.

As far as the inlet and outlet boundary conditions are concerned, the spirit of the classical lambda formulation has been preserved.[3] On the contrary, the impermeability condition at the solid wall has been enforced by means of the symmetry technique proposed and tested in Ref. 15.

The extension of the present procedure to the computation of the Navier-Stokes equations requires the consideration of additional terms, corresponding to the heat flux and shear stress contributions, which can be computed in a strict finite-volume fashion in the same way they are treated by classical conservative finite-volume methodologies.

Shock Computation

The insertion of the lambda formulation approximation in the computation of the finite-differences in Eq. (16), together with the separation of the contributions due to fluxes and geometry variations in Eq. (14), gives a nonconservative discretization of Eq. (4), which is appropriate to compute smooth flow regions with a high accuracy. As a counterpart, no discontinuity can be captured by the present formulation, because of the loss of the conservation property.

Such a property can be easily recovered near discontinuities, following the basic idea suggested in Ref. 9, which has been adapted to the present situation and put to work in Ref. 12. Practically, it brings us to switch from the previously outlined nonconservative discretization, in smooth flow regions, to a conservative formulation and scheme near discontinuities, where the flux difference splitting technique suggested by Roe[16] has been used. The flux limiters, employed by upwind conservative schemes, can be used to detect such discontinuities and to trigger the conservative-nonconservative change. Indeed, the authors have experienced efficient discontinuity detections by employing the well known minmod limiter.[14] Alternatively, the discontinuities detection techniques suggested by Moretti[2,3] can be used: these are essentially based on finding discontinuities in eigenvalues. Whichever kind of detection device is used, an automatic switch between nonconservative and conservative discretization schemes can be easily obtained, so that all the requirements stated in the introduction are finally satisfied with the exception of the classical lambda formulation accuracy preservation, which will be checked by means of some numerical experiments.

At this stage we may observe the present formulation is suitable for a discontinuity fitting procedure too, when it is required. In such a case a discontinuity tracking procedure must be worked out following the guidelines given in Refs. 2–6.

Results

One-dimensional cylindrical and spherical source flows have been analyzed in Ref. 12 and computed by means of Cartesian meshes, in order to obtain simple two- and three-dimensional flows with an exact solution, for comparison of the results. In particular, shockless subsonic and supersonic flows have been computed by means of the present formulation as well as Roe's flux difference splitting methodology. The corresponding mean square errors with respect to the exact solution have been evaluated. A comparison of such errors, reported in Ref. 13, outlines that the proposed formulation accuracy is superior to Roe's scheme accuracy by a factor ranging between 2.5–5. As far as the computational time is concerned, the present formulation is about two times faster than Roe's scheme, when the same number of mesh intervals are used. Taking into account that doubling the number of mesh intervals in each direction requires halving the time step, we may conclude that the use of Roe's scheme implies a computational time about 30 times longer, in order to compute three-dimensional subsonic or supersonic source flow results with the same level of accuracy. Although such a conclusion is limited to the considered test cases, one can reasonably state the present formulation requires computational times one order of magnitude lower than the ones needed by Roe's scheme, if the same global accuracy is wanted. The above outlined results prove the superior accuracy and computational efficiency of the proposed formulation with respect to a flux difference splitting technique.

In order to prove that the present technique and the classical lambda formulation are characterized by a comparable accuracy, the two-dimensional subsonic flow inside a plane channel with a circular bump has been considered: the ratio of the channel width to the circular arc chord is equal to 1, while the ratio of the circular arc height to such a chord is equal to 0.1. The mesh employed in the present computation is made by 33 × 10 cells. A high Mach number subsonic flow case, corresponding to a downstream isentropic Mach number equal to 0.52, has been considered. The computed pressure coefficient distribution on the bump surface is plotted in Fig. 1 (symbols), together with the corresponding results (continuous line) obtained by means of a code developed according to the classical lambda formulation.[4] Moreover, the computed isobar pattern is reported in Fig. 2. The results shown in Figs. 1 and 2 outline a very good symmetry between the inlet and the outlet flow regions, as it should be, because of the geometrical symmetry and the subsonic nature of the flow. Moreover, in spite of the coarse grid employed, Fig. 1 shows a very good agreement between the results computed by means of the suggested technique and the classical lambda formulation. In the present flow case, no exact solution exists, so that a deeper accuracy analysis can only evaluate the total pressure and total temperature errors and the symmetry errors between the inlet and outlet regions, i.e., the differences between the values of physical variables at two points symmetrically located with respect to the vertical symmetry line. Such an error analysis has been performed in Ref. 13 and has proven the

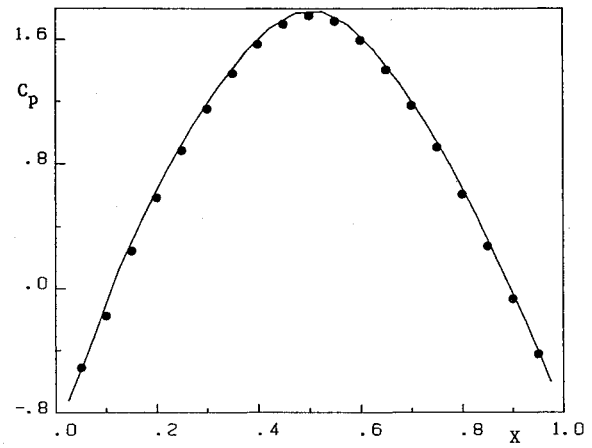

Fig. 1 Bump channel subsonic flow: pressure coefficient on the bump surface (continuous line: reference results from Ref. 4; dark circles: present results).

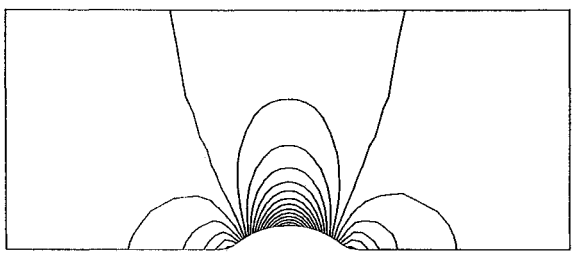

Fig. 2 Bump channel subsonic flow: isobar contours.

slightly superior accuracy of the finite-volume lambda formulation in comparison with the classical lambda formulation.

The second considered two-dimensional flow case is the shockless transonic flow inside the Hobson Cascade 1,[17] a symmetric cascade characterized by an exact hodograph solution. Such a test case is very severe because the flow solution is singular in the sense that small perturbations in incident Mach number and angle can lead to flow patterns with shocks. The flow main characteristics are an inlet and outlet critical Mach number equal to 0.51 and inlet and outlet angles equal to 43°.544 and −43°.544, respectively. Computations have been performed by means of two different nonorthogonal meshes, made by 28 × 10 and 46 × 19 cells, 11 and 21 cells being located on the cascade suction side, respectively. Figure 3 presents the exact critical Mach number on the cascade surface (continuous line) together with the computed solutions (dark circles and light squares refer to the finer and coarser mesh, respectively), while Fig. 4 shows the computed isoMach contours. Figure 3 shows a good agreement between the computed and exact results, for the coarser mesh solution too. It also proves that the computed results lead to the exact ones when the mesh is refined. Moreover, Fig. 4 demonstrates the good symmetry of computed results. The reliability and robustness of the suggested methodology have also been proven by the following numerical experiments. The flow inside the Hobson cascade has been computed by means of different mesh patterns and sizes: slightly different mesh dependent solutions have been obtained, but none of them has led to flow patterns with shocks.

Two subsonic three-dimensional test cases have then been considered. The first one is the flow inside an accelerating rectangular elbow, designed by Stanitz[18] and originally introduced to test some aspects of secondary flow development in a turbine vane, i.e., the passage vortex formation and intensification in a contracting curved duct.[19] Some very accurate experimental results have been recently reported in Ref. 20. The configuration, shown in Fig. 5, has been experimentally tested with a thickened end wall boundary layer, obtained by means of an upstream spoiler. In the present computations a

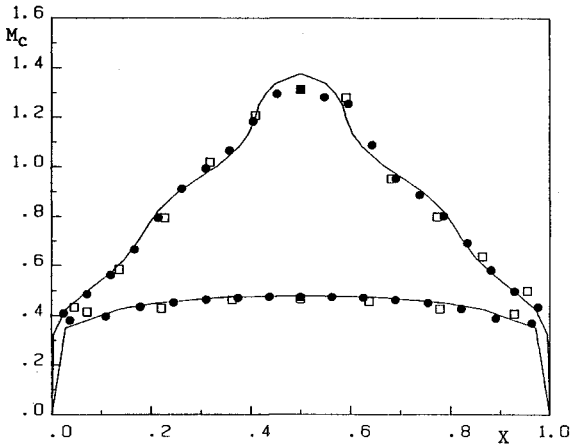

Fig. 3 Hobson cascade 1: surface critical Mach number distribution (continuous line: exact solution; dark circles: 46 × 19 cells; light squares: 28 × 10 cells).

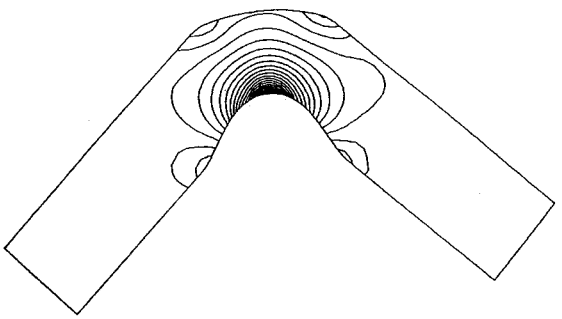

Fig. 4 Hobson cascade 1: isoMach contours.

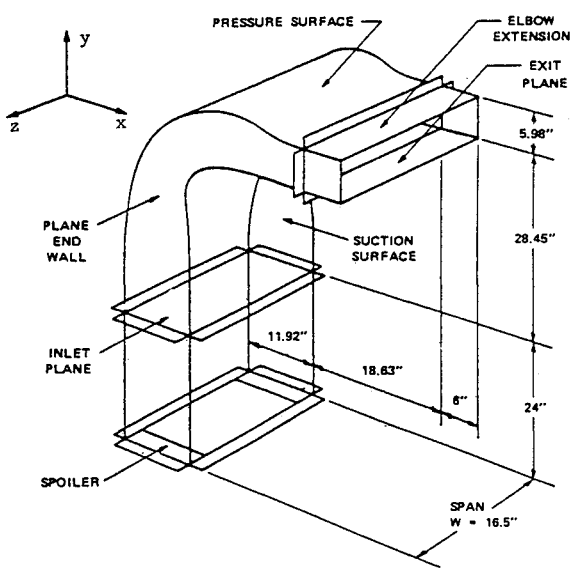

Fig. 5 Schematic of Stanitz accelerating rectangular elbow.

quasiorthogonal grid, made by 30 × 10 × 15 cells, has been employed to describe only one-half of the duct, because of the flow symmetry with respect to the midspan. Figure 6, taken from Ref. 20, presents the pressure coefficient around the duct periphery at selected axial stations. According to Stanitz, the pressure coefficient has been defined as

$$C_p = (p - p_a)/(p_T - p_a) \tag{20}$$

In Fig. 6, suction surface results correspond to abscissa values between zero and one, end wall results to values between one and two, and pressure surface results to values between two and three. The lowest value represents the axial station closest

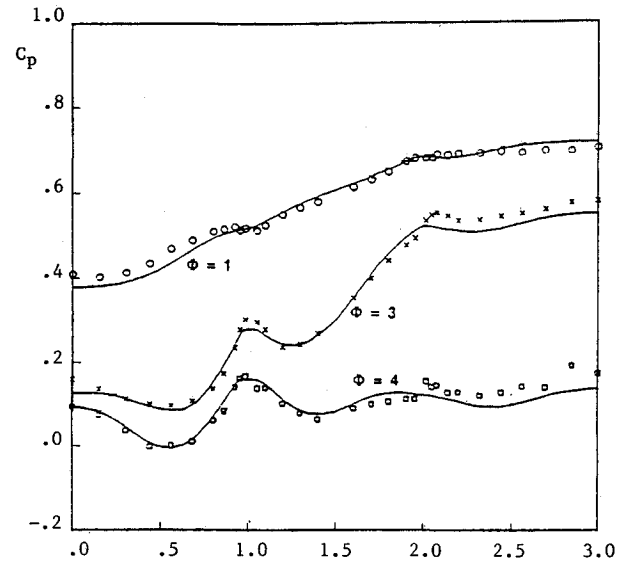

Fig. 6 Stanitz elbow: pressure coefficient distributions around the duct periphery at selected axial stations from Ref. 20 (continuous lines: computed viscous results; symbols: experimental data).

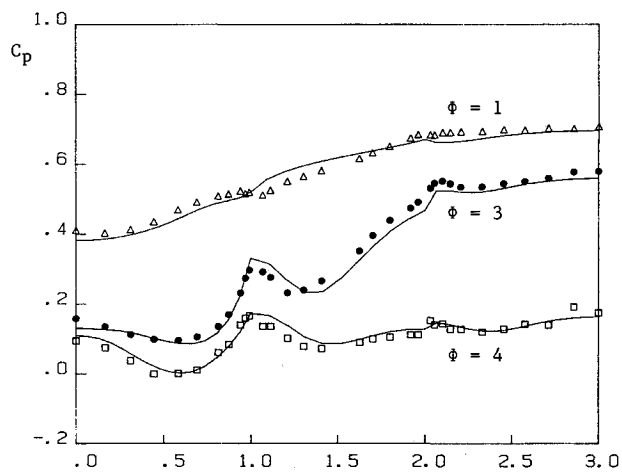

Fig. 7 Stanitz elbow: present pressure coefficient distribution around the duct periphery at selected axial stations (continuous lines: computed results; symbols: experimental data).

to the inlet plane, while the highest value refers to the station closest to the outlet plane. The experimental data, corresponding to a nominal mainstream exit Mach number equal to 0.45, are given as symbols, while the continuous lines refer to the results computed in Ref. 20 by means of a viscous code. Figure 7 presents the corresponding results computed in accordance with the present formulation. The agreement between theoretical and experimental results in Fig. 6 is as good as in Fig. 7, thus outlining that the present formulation can compute wall static pressure as accurately as a viscous formulation, at least as the one suggested in Ref. 20.

In Ref. 20, experimental total pressure contours at the elbow exit plane are also given. Such experimental results are shown in Fig. 8 as contours of constant total pressure loss (ΔP_t) defined as

$$\Delta P_t = (p_T - p_t)/(p_T - p_a) \tag{21}$$

The corresponding contours, computed by means of the present formulation, are plotted in Fig. 9. The present results give the main feature of the experimental total pressure loss contours and compare with them much better than other published inviscid results. However, some discrepancies between computed and experimental results can be found: the boundary layer on the pressure surface cannot be computed, the midspan results to be a no-loss surface. These discrepancies are characteristic of any accurate inviscid calculation. Indeed, in steady inviscid flows the total pressure is constant along streamlines; being the midspan surface a stream surface characterized by no total pressure loss at the inlet, no total pressure loss must be computed at the outlet by any accurate inviscid code, as it is the case in the present computation. The boundary layer at the pressure side and the midspan losses are typical viscous effects which cannot be reproduced by accurate inviscid formulations.

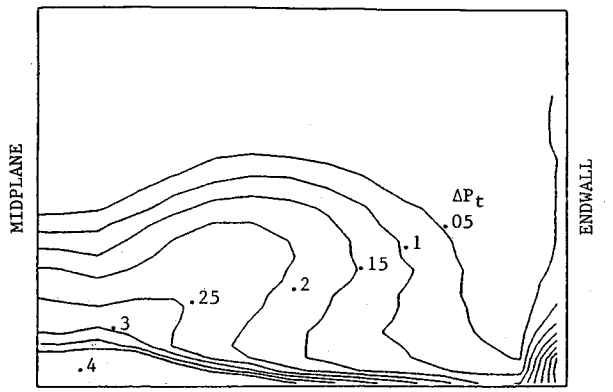

Fig. 8 Stanitz elbow: experimental exit total pressure loss contours.[20]

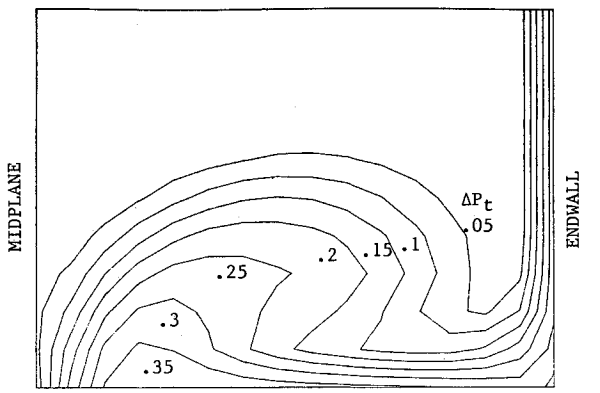

Fig. 9 Stanitz elbow: present numerical exit total pressure loss contours.

The second considered subsonic three-dimensional flow case is the test case E/CA-7, suggested in Ref. 21 for inviscid calculations too. It is a cascade of turbine blades with side walls presenting a 6°.26 divergence in the blade passage. At the design condition here considered, this cascade has an exit isentropic Mach number of 0.71 and an incidence angle of 38.8 deg. The computation of such a test case has been performed by using only 25 × 9 × 7 cells. The computed midspan surface isentropic Mach number distribution is plotted in Fig. 10 (symbols) together with the corresponding experimental data (continuous line), while Fig. 11 shows the midspan isobar contours inside the cascade. Taking into account the inviscid nature of the present formulation, the agreement between computed and experimental results in Fig. 10 can be considered quite satisfactory, with the exception of the leading-edge region where the present coarse mesh cannot accurately describe the stagnation point flow features. This same test case has been considered in Ref. 22 and computed by means of an inviscid formulation and using a much finer 80 × 16 × 16 mesh: the reported agreement between computed isentropic Mach number and experimental data compares very well with the present one (Fig. 10), in particular as refers to the blade upper surface; moreover, the reported isobar contours agree with those plotted in Fig. 11, with the obvious exception of the leading-edge region.

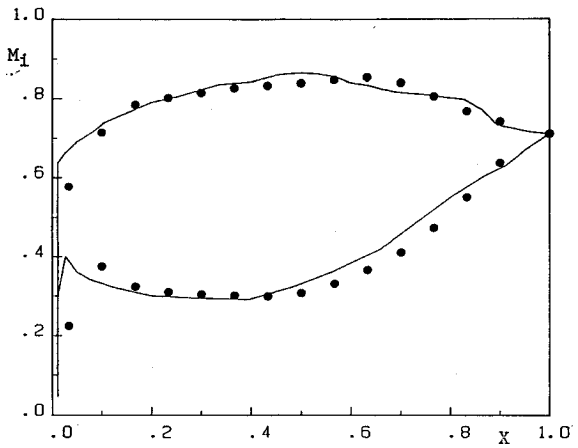

Fig. 10 Test case E/CA-7: midspan surface isentropic Mach number distribution (continuous lines: experimental data; dark circles: 25 × 9 × 7 cells).

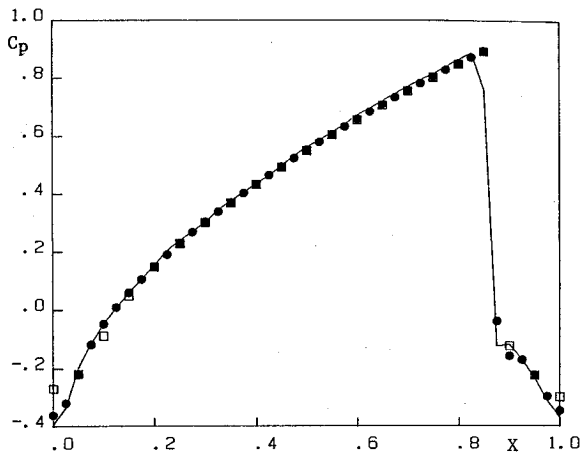

Fig. 12 Bump channel transonic flow: pressure coefficient distribution on the bump surface (continuous line: reference results from Ref. 24; dark circles: 63 × 24 cells; light squares: 31 × 12 cells).

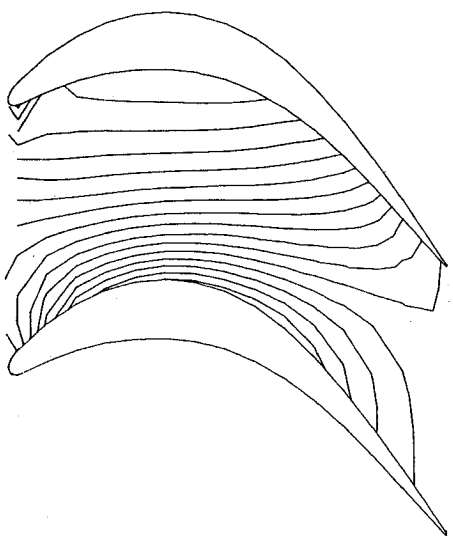

Fig. 11 Test case E/CA-7: midspan isobar contours.

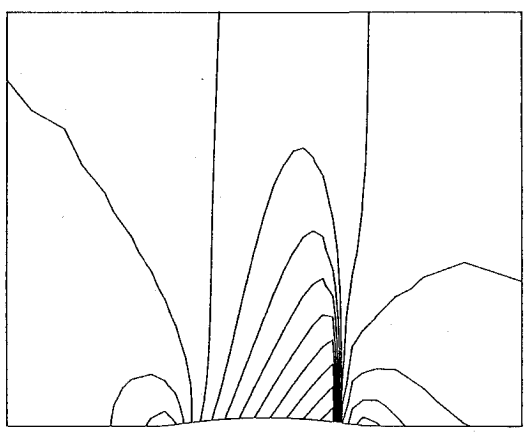

Fig. 13 Bump channel transonic flow: isoMach contours.

Finally, two transonic test cases have been considered: 1) a two-dimensional and 2) a three-dimensional flow case. The two-dimensional one is the classical transonic flow inside a plane channel with a circular bump[23] and characterized by a downstream isentropic Mach number equal to 0.85. The height to chord ratio of the circular arc is equal to 0.042 and the ratio of the channel width to such a chord is equal to 2.073. Computations have been performed by means of two different nonorthogonal meshes with 31 × 12 and 63 × 24 cells. The steady-state pressure coefficient results at the bump surface are plotted in Fig. 12: the dark circles and the light squares refer to the results computed by means of the finer and the coarser mesh, respectively; the continuous line represents the reference results given by Montagné[24] and computed by using a flux difference splitting methodology and 72 × 21 grid-points. In spite of the completely different type of employed methodologies, Fig. 12 outlines a very good agreement between the present results and the reference ones, in particular as refers to the shock position. Such an agreement proves the very good accuracy of the present results computed by means of a very coarse mesh (only 31 × 12 cells), with some obvious differences in the leading- and trailing-edge regions, which do not affect the overall accuracy. Finally, the isoMach contours computed by means of the coarser mesh are plotted in Fig. 13. A comparison of such results with the corresponding contours computed by means of the classical lambda formulation supplemented by a shock-fitting technique (see Fig. 10 in Ref. 4) outlines the practical coincidence of the two sets of results. Such a comparison, together with the conclusions drawn from Fig. 12, proves the reliability of the present formulation for transonic flow computations too.

In order to test the proposed methodology in three-dimensional transonic flow conditions too, the following simple steady one-dimensional spherical source flows, already suggested in Ref. 12, have been considered:

$$\begin{aligned} a^5 v_r r^2 &= k \\ 0.2 v_r^2 + a^2 &= 1.4 \end{aligned} \tag{22}$$

Equation (22) represents one-dimensional flows when a spherical coordinate system is used, while they represent three-dimensional flows if a Cartesian coordinate system is employed. In such a way, simple three-dimensional flows can be devised which are characterized by a known exact solution, for comparison of the computed results. In order to get a transonic flow test case, an unshocked value of k and the prescribed shock position must be defined, which determine the flow conditions upstream of the shock. The downstream flow conditions are then determined by the shocked value of k, which can be evaluated by taking use of the Rankine-Hugoniot conditions. We have considered the transonic flow corresponding to an unshocked value of k equal to 1.0 and to a prescribed shock located at $r = 2.4$. Such a flow case has been computed by means of two different Cartesian meshes, employing a maximum of 12 and 25 cells in each direction. The channel geometry is represented in Fig. 14, while Fig. 15 presents the pressure distribution vs the radial distance from the origin, along the main diagonal, i.e., the line AB in

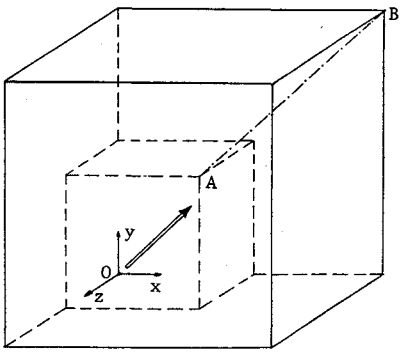

Fig. 14 Three-dimensional source flow: geometry.

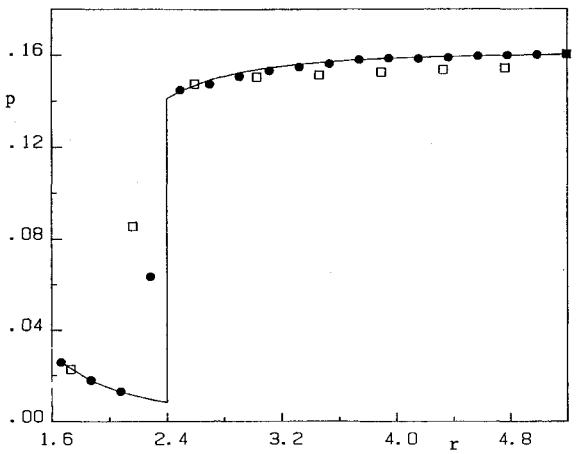

Fig. 15 Three-dimensional source flow: pressure distribution along the main diagonal (continuous line: exact solution; dark circles: finer mesh; light squares: coarser mesh).

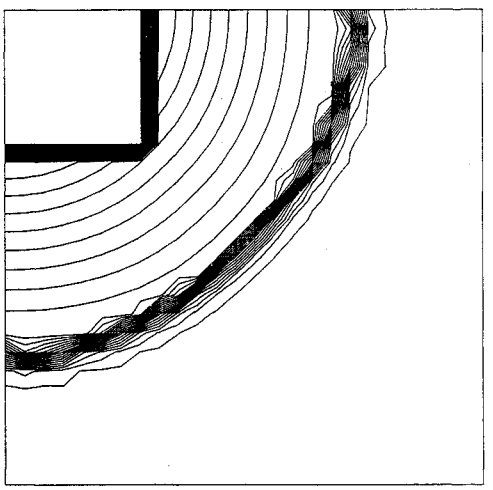

Fig. 16 Three-dimensional source flow: logarithmic pressure contours.

Fig. 14 (the continuous line shows the exact solution, while the dark circles and the light squares represent the results computed with the finer and the coarser mesh, respectively). Moreover, Fig. 16 shows the logarithmic pressure contours computed by means of the finer mesh and corresponding to the x-y plane at one-fourth of the channel dimension in the z direction. A quick glance to Figs. 15 and 16 brings us to the following conclusions: the results computed by means of the two meshes are sufficiently close, with the obvious exception of the shock transition region; the results computed by means of the finer mesh agree very well with the exact solution; the shock is correctly located; the shock position and the computed results tend to the exact values when increasing the cell number; the isobar contours are circles or very close to circles, as they should be. Such conclusions prove once more the reliability of the proposed methodology.

Conclusions

A finite-volume lambda formulation for the computation of inviscid flows has been presented which satisfies the following requirements: the equations are discretized in nonconservative form in smooth flow regions, in order to take advantage of its superior accuracy; the discretization scheme automatically switches to conservative form near discontinuities, to preserve the discontinuity capturing capability of such schemes; the same dependent variables are employed in the whole flowfield, independently on the local form of the discretization scheme; the formulation is in finite-volume form, in order to easily describe complex geometries. The suggested formulation can also be easily extended to the computation of Navier-Stokes equations, as briefly shown. Computations of some two- and three-dimensional flow test cases have proven the superior accuracy and computational efficiency of the proposed formulation, in comparison with a classical conservative upwind methodology. Moreover, some computations have outlined the suggested formulation slightly improves the superior accuracy of the classical lambda formulation. Comparison of computed results with exact, numerical or experimental published ones has shown the capability of the finite-volume lambda formulation to deal with subsonic as well as transonic flow cases and the reliability of computed results. The present formulation must be tested in more complex three-dimensional geometries, to prove its applicability to problems of greater engineering interest. Moreover, following the suggested guidelines, viscous terms must be inserted in order to extend the formulation applicability to the computation of viscous flows.

Acknowledgment

The present research has been supported by the Italian Agency Ministero dell' Universita' e della Ricerca Scientifica e Tecnologica (MURST 40%).

References

[1]Moretti, G., "The λ-Scheme," *Computers and Fluids*, Vol. 7, No. 2, 1979, pp. 191–205.

[2]Moretti, G., "A Technique for Integrating Two-Dimensional Euler Equations," *Computers and Fluids*, Vol. 15, No. 1, 1987, pp. 59–75.

[3]Dadone, A., and Moretti, G., "Fast Euler Solver for Transonic Airfoils," *AIAA Journal*, Vol. 26, April 1988, pp. 409–425.

[4]Dadone, A., Fortunato, B., and Lippolis A., "A Fast Euler Solver for Two- and Three-Dimensional Internal Flows," *Computers and Fluids*, Vol. 17, No. 1, 1989, pp. 25–37.

[5]Moretti, G., "An Efficient Euler Solver, with Many Applications," *AIAA Journal*, Vol. 26, June 1988, pp. 655–660.

[6]Dadone, A., and Fortunato, B., "Three-Dimensional Flow Computations with Shock Fitting," AIAA Paper 90-0109, Jan. 1990.

[7]Dadone, A., and Magi, V., "A Quasi-Conservative Lambda Formulation," *AIAA Journal*, Vol. 24, Aug. 1986, pp. 1277–1284.

[8]Pandolfi, M., "The Merging of Two Different Ideas: A Shock Fitting Performed by Shock Capturing," International Symposium on Computational Fluid Dynamics, Tokyo, Sept. 1985.

[9]Favini, B., and Zannetti, L., "On Conservative Properties and Non-Conservative Forms of Euler Solvers," *Lecture Notes in Physics*, Vol. 264, 1986, pp. 270–275.

[10]Godunov, S. K., "A Finite Difference Method for the Numerical Computation of Discontinuous Solutions of the Equations of Fluid Dynamics," *Mathematik Sbornik*, Vol. 47, 1959, pp. 271–306.

[11]Dadone, A., and Vacca, G., "Calcolo di Flussi Transonici Mediante Formulazione Lambda Conservativa," *Proceedings of 44 Congresso Nazionale ATI*, Vol. 5, 1989, pp. 47–55.

[12]Dadone, A., "A Conservative Lambda Formulation," *Proceedings of the Third International Conference on Hyperbolic Problems*, Uppsala Univ., Dept. of Scientific Computing and Studentlitteratur, Uppsala, Sweden, Vol. 1, 1991, pp. 270–284.

[13]Casalini, F., and Dadone, A., "A Finite Volume Lambda Formulation," AIAA Paper 91-2258, June 1991.

[14]Walters, R. W., and Thomas, J. L., "Advances in Upwind Relaxation Methods," *State-of-the-Art Survey on Computational Mechanics*, edited by A. K. Noor, American Society of Mechanical Engineers, New York, 1988.

[15]Dadone, A., "A Physical-Numerical Treatment of Impermeable Boundaries in Compressible Flow Problem," *Proceedings of the Fourth International Symposium on Computational Fluid Dynamics*, Davis, CA, Sept. 1991, Vol. 1, pp. 258–263.

[16]Roe, P. L., "Characteristic-Based Schemes for the Euler Equations," *Annual Review of Fluid Mechanics*, Vol. 18, 1986, pp. 337–365.

[17]Hobson, D. E., "Shock-Free Transonic Flow in Turbomachinery Cascade," Cambridge Univ. Engineering Dept., Paper CUED/A TURBO/TR65, 1974.

[18]Stanitz, J. D., "Design of 2-D Channels with Prescribed Velocity Distributions Along the Channel Walls, *I*—Relaxation Solution," NACA TN 2593, Jan. 1952.

[19]Stanitz, J. D., Osborn, W. M., and Mizisin, J., "An Experimental Investigation of Secondary Flows in an Accelerating, Rectangular Elbow with 90° of Turning," NACA TN 3015, Oct. 1953.

[20]Kreatsoulas, J. C., Lee, D., and Ballantine, A., "Experimental/Computational Study of Viscous Flow in an Accelerating, 90 Degree, Rectangular Elbow," AIAA Paper 88-0186, Jan. 1988.

[21]Agard Propulsion and Energetics Panel, "Test Cases for Computation of Internal Flows in Aero Engine Components," edited by L. Fottner, AGARD AR 275, 1990.

[22]Liu, F., and Jameson, A., "Multigrid Euler Calculations for Three-Dimensional Cascades," AIAA Paper 90-0688, Jan. 1990.

[23]Rizzi, A., and Viviand, H. (eds.), "Numerical Methods for the Computation of Inviscid Transonic Flows with Shock Waves: A GAMM Workshop," Vieweg, Braunscheig, 1981.

[24]Montagné, J. L., "A Second-Order Accurate Flux-Splitting Scheme in Two-Dimensional Gasdynamics," *Lecture Notes in Physics*, Vol. 218, 1985, pp. 406–411.